Journal of Power Sources 249 (2014) 148–155

Contents lists available at ScienceDirect

Journal of Power Sources

journal homepage: www.elsevier.com/locate/jpowsour

Layer-by-Layer assembled hybrid multilayer thin film electrodes based on transparent cellulose nanofibers paper for flexible supercapacitors applications

Xi Wang [a,b], Kezheng Gao [a,b], Ziqiang Shao [a,b,*], Xiaoqing Peng [a,b], Xue Wu [a,b], Feijun Wang [a,b]

[a] School of Materials Science & Engineering, Beijing Institute of Technology, Beijing 100081, PR China
[b] Beijing Engineering Research Center of Cellulose and Its Derivatives, Beijing Institute of Technology, Beijing 100081, PR China

HIGHLIGHTS

- Cellulose nanofibers paper was used as the substrates for supercapacitors.
- Layer-by-Layer assembly method was used to create highly tunable thin films.
- The properties of hybrid electrodes with diverse microstructures were studied.
- The value of effective pathway for ion transportation was demonstrated.
- We report a method to prepare electrodes for future flexible supercapacitors.

ARTICLE INFO

Article history:
Received 15 August 2013
Received in revised form
27 September 2013
Accepted 30 September 2013
Available online 25 October 2013

Keywords:
Supercapacitor
Layer-by-Layer assembly
Cellulose nanofibers
Hybrid thin film electrodes
Ion diffusion

ABSTRACT

Cellulose nanofibers (CNFs) paper with low thermal expansion and electrolyte absorption properties is considered to be a good potential substrate for supercapacitors. Unlike traditional substrates, such as glass or plastic, CNFs paper saves surfaces pretreatment when Layer-by-Layer (LbL) assembly method is used. In this study, negatively charged graphene oxide (GO) nanosheets and poly(3,4-ethylenedioxythiophene: poly(styrene sulfonate)) (PEDOT:PSS) nanoparticles are deposited onto CNFs paper with positively charged polyaniline (PANI) nanowires as agents to prepare multilayer thin film electrodes, respectively. Due to the different nanostructures of reduced graphene oxide (RGO) and PEDOT:PSS, the microstructures of the electrodes are distinguishing. Our work demonstrate that CNFs paper/PANI/RGO electrode provides a more effective pathway for ion transport facilitation compared with CNFs paper/PANI/PEDOT:PSS electrode. The supercapacitor fabricated by CNFs/$[PANI–RGO]_8$ (S-PG-8) exhibits an excellent areal capacitance of 5.86 mF cm^{-2} at a current density of 0.0043 mA cm^{-2}, and at the same current density the areal capacitance of the supercapacitor fabricated by CNFs/$[PANI–PEDOT:PSS]_8$ (S-PP-8) is 4.22 mF cm^{-2}. S-PG-8 also exhibits good cyclic stability. This study provides a novel method using CNFs as substrate to prepare hybrid electrodes with diverse microstructures that are promising for future flexible supercapacitors.

1. Introduction

Nowadays, transparent flexible energy storage devices, especially supercapacitors, have attracted a lot of attentions [1–6]. The substrates play an important role in fabricating supercapacitors, because they are crucial for the basic characteristics of the devices. Traditional substrates such as ITO-coated glass, polyethylene terephthalate (PET), polyethylene naphthalate (PEN), polycarbonate (PC), and polyimide (PI) have been used [7–10]. However, several properties of them are unsatisfactory, including inflexibility, large coefficient of thermal expansion (CTE), poor printability and recyclability. Recently, new biodegradable, flexible, and transparent cellulose nanofibers (CNFs) paper may reach our expectation due to its excellent optical transmittance (above 90% in visible region), low CTE (about 2.7 ppm K^{-1}), high mechanical strength, excellent flexibility and the plywood-like hierarchical structure [11,12]. Due

* Corresponding author. Beijing Engineering Research Center of Cellulose and Its Derivatives, Beijing Institute of Technology, Beijing 100081, PR China. Tel.: +86 010 68941797x601; fax: +86 010 68941797x609.
E-mail addresses: 95473104@qq.com (X. Wang), gaokezheng@163.com (K. Gao), shaoziqiang@263.net (Z. Shao).

0378-7753/$ – see front matter © 2013 Published by Elsevier B.V.
http://dx.doi.org/10.1016/j.jpowsour.2013.09.130

to the carboxylic acid groups, CNFs paper has a net negative charge in aqueous solution. It is a convenient condition for Layer-by-Layer (LbL) assembly, which avoids the troubles carried by the surfaces pretreatment of traditional uncharged substrates.

LbL assembly allows the incorporation of diverse nanostructures, including nanotubes, nanosheets, nanoparticles and biomolecules with nanofibers [13]. Using LbL assembly method to combine nano-scale active materials with CNFs paper, can not only create highly tunable, conformal thin films [14], but also maintain the functional surfaces with nano-scale composition and structure [15], which is significant for the performance of supercapacitors. Moreover, due to the random orientation of CNFs during paper formation, the CNFs paper's surface is rugged, which shows a "water waves-like" texture (Fig. S1a in the ESI). So CNFs paper may act as aqueous electrolyte nano-reservoirs when it used as a part of electrodes in supercapacitors.

Polyaniline (PANI) is one of the most technologically promising electrically conducting polymers (ECPs) used for electrode materials with its excellent pseudocapacitive behavior, low cost, ease of synthesis and interesting redox properties [2,16,17]. It has four redox states with distinct colors, including leucoemeraldine base (LB, yellow), emeraldine salt (ES, green), emeraldine base (EB, blue) and pernigraniline base (PB, purple) [16,18]. The EB form can be easily doped into the conductive and electrochemically active ES form with positive charges at low pH values (pH < 3). Thus, it can be deposited on the surface of CNFs paper by electrostatic interaction. In this study, PANI nanowires (ES form) were prepared to be used as agents to combine CNFs paper with negatively charged active material. And then, multilayer film electrodes were prepared by LbL assembly. Furthermore, owing to interesting electrochromic properties of PANI, the supercapacitors fabricated by the multilayer films may be electrochromic [8,16,19].

Graphene oxide (GO) and poly(3,4-ethylenedioxythiophene: poly(styrene sulfonate)) (PEDOT:PSS) are widely used to prepare electrodes [20–23]. Both of them are negatively charged in aqueous solution, so they can be used as the other kind of active material mentioned above. However, the structures of them are totally different, graphene oxide (GO) is nanosheet, and PEDOT:PSS is nanoparticle in aqueous solution. The dissimilar microstructure may impact the properties of the supercapacitors. GO nanosheets are almost non-conducting and they can be transformed from their insulating state to conductive state (reduced graphene oxide (RGO) nanosheets) by the chemical reduction [24]. The aggregation of GO nanosheets during the reduction process is inevitable, which will decrease the performance of RGO-based supercapacitors [25]. If these GO nanosheets are assembled with conductive PANI nanowires on the substrate using LbL assembly technique under electrostatic interaction, and then the GO nanosheets are reduced to RGO nanosheets, the compact stacking of RGO nanosheets (the structural characteristics of graphite) may be effectively prevented by these nanowires. The conductive PANI nanowires can also act as active material to drop vertical resistivity of the multilayer thin film electrodes, and the pseudocapacitive behavior of PANI may make up for the deficiency of the low capacitance of RGO. Moreover, the interspace between RGO nanosheets layers and PANI nanowires may effectively facilitate diffusion of electrolyte ions [26].

PEDOT has emerged as one of the most widely used ECPs, due to its relatively high electrical conductivity and better environmental stability compared with other ECPs [27]. However, PEDOT' insolubilization limits its application. After doped with PSS, the dissolvability of PEDOT has been improved. PEDOT:PSS has been used as transparent conductive layer in supercapacitors [21,28]. Because of the better transparency of PEDOT:PSS, the electrodes made from PEDOT:PSS, PANI and CNFs paper may more transparent than that made from RGO, PANI and CNFs paper. However, PEDOT:PSS nanoparticles and PANI nanowires may form a dense compact structure, which will block the diffusion of electrolyte ions.

Some efforts have been made to investigate the properties of PANI incorporated with GO nanosheets or PEDOT:PSS. However, CNFs, PANI and PEDOT:PSS (or RGO) multilayer films made by LbL assembly method, and the applications of the supercapacitors based on these multilayer film electrodes have not been reported yet. A comprehensive comparison of the supercapacitors made from nanocomposite film electrodes with different microstructure has not been reported, too.

In our work, CNFs/$[PANI\text{-}GO]_n$ (hereafter CPG-n, n is the number of bilayers) films and CNFs/$[PANI{-}PEDOT{:}PSS]_n$ (hereafter CPP-n) films were prepared by LbL assembly method. Before fabricating the supercapacitors, the CPG-n films were transformed to conductive CNFs/$[PANI{-}RGO]n$ (hereafter CPRG-n) films by the chemical reduction with hydroiodic (HI) acid. A comparison of the supercapacitors fabricated by CPRG-n films and CPP-n films is reported. The results indicate that the CPRG-8-based supercapacitor possesses outstanding electrochemistry performance and the CPP-8-based supercapacitor is more transparent.

2. Experimental

2.1. Materials

Hardwood bleached kraft pulps in the never-dried wet state with 78% water content, 2,2,6,6-tetramethylpiperidine-1-oxyl radical (TEMPO), sodium bromide, sodium hypochlorite solution, ammonium peroxydisulfate (APS), aniline, ammonium hydroxide, dimethylacetamide (DMAc), graphite powder (200–325 mesh), concentrated sulfuric, potassium peroxodisulfate, phosphorus pentoxide, potassium permanganate, hydrogen peroxide, 3,4-ethylenedioxythiophene (EDOT), poly(styrene sulfonate) (PSS), ferric sulfate. 3,4-Ethylenedioxythiophene and poly(styrene sulfonate) were purchased from Energy Chemical, and the others were purchased from Beijing Chemical Reagents Company with their purity being of analytical grade. Aniline and 3,4-ethylenedioxythiophene were distilled under reduced pressure prior to use. The other chemicals were used without further purification.

2.2. Preparation of CNFs paper

CNFs suspension was prepared according to the literature method reported by Isogai [29], and described in brief as follows: TEMPO (0.033 g) and sodium bromide (0.33 g) were dissolved in deionized water (400 mL) with continuous stirring. Hardwood bleached kraft pulps (2 g) were added after the catalysts have been completely dissolved. The oxidation reaction was started by adding the desired amount of the NaClO solution (15 mmol g^{-1} cellulose). 0.5 M NaOH was added to maintain the pH of the reaction solution at about 10.00–10.50 at 10 °C for 6 h. The TEMPO-oxidized cellulose was washed thoroughly with deionized water by filtration. 2 mg mL^{-1} oxidized cellulose/water slurries were sonicated for 15 min at power of 300 W in an ice bath. Transparent CNFs dispersion was prepared by centrifuging at 10,000 rpm for 10 min to remove the unfibrilated cellulose. The transparent CNFs dispersion was used to prepare CNFs paper by pouring practice. The detailed characterization of CNFs and CNFs paper is provided in the supplementary material (Fig. S1b, c and d).

2.3. Preparation of PANI, GO and PEDOT:PSS suspension

The synthesis of PANI suspension was based on a previously reported method [19,30,31] (ESI). Dispersions of GO were produced using a modified Hummers' method [32] from graphite powder

(see the ESI for details). The PEDOT:PSS suspension is prepared as follows: APS (0.68 g) and ferric sulfate (0.0016 g) were dissolved in water (400 mL). PSS (0.82 g) was dissolved in water (40 mL) with continuous stirring. EDOT (0.28 g) was added after the PSS had been completely dissolved. Successively, the pH value was further lowered to 2–3 by adding several drops of 1 M HCl. The oxidation reaction was started by adding the mixture of APS and ferric sulfate. The solution was stirred for 24 h at room temperature. The remaining salt impurities were removed by treating with resinous anion and cation exchangers. The microstructure of PANI, GO and PEDOT:PSS was investigated with transmission electron microscopy (TEM), which provided in the supplementary material (Fig. S2a, b and c).

2.4. Preparation of hybrid multilayer thin film electrodes

The CPP-*n* and CPG-*n* films were assembled using the procedure shown in Scheme 1, and described in brief as follows. Each CNFs films was first immersed in the PANI dipping solution for 3 min, washed with deionized water and a HCl aqueous solution (pH value = 2.6–2.9), and dried with an air stream. Then, the PANI coated CNFs film was immersed in the PEDOT:PSS (or GO) dipping solution for 3 min, followed by washing with deionized water and dried through the same procedure. Multilayer films were grown by cyclic immersion in positively charged PANI solutions and negatively charged PEDOT:PSS (or GO) solutions. Successively, the multilayer films CPG-*n* were reduced by immersing in HI acid (90 °C) for 10 s [33]. Here, HI acid was selected as the reducing agent to yield conductive reduced graphene oxide layers with good integrity and flexibility. Finally, the CPRG-*n* films were washed by water and dried in air.

2.5. Preparation of the flexible thin film supercapacitors

Scheme 1 also shows the processes of fabricating the flexible thin film supercapacitors. They are assembled by two hybrid paper in a traditional two-electrode stacked configuration, the H_2SO_4–polyvinyl (PVA) gel is chosen as the electrolyte and it is also used as separator simultaneously performs [34]. The supercapacitor fabricated by CPRG-8 films is named S-PG-8, and fabricated by CPP-8 films is called S-PP-8.

2.6. Materials characterization

Ultraviolet–visible (UV–vis) absorption spectra were recorded on a Lambda 35 UV–vis spectrometer (Perkin Elmer Instruments Co. Ltd., USA). X-ray photoelectron spectroscopy (XPS) of the samples was performed on a PHI 5300 Photoelectron Spectrometer (Perkin Elmer Instruments Co. Ltd., USA). X-ray diffraction (XRD) analysis was carried out with a Bruker AXS D8 Discover diffractometer (Germany) using Cu-Kα radiation (λ = 1.5406 Å). The 2θ range used in the measurements was from 10 to 30°. Scanning electron microscopy (SEM) was conducted using a Hitachi S-4800 field-emission-gun scanning electron microscope (Japan) at 5.0 kV.

2.7. Electrochemical characterization

The electrochemical performances of the S-PG-8 and S-PP-8 were evaluated on a CHI 660E electrochemical workstation (CH Instruments Inc.). All the measurements were carried out in air at room temperature. Cyclic voltammograms were recorded from −0.2 to 0.8 V at scan rates of 2, 5, 10, 50 and 100 mV s^{-1}. The galvanostatic charge–discharge (GCD) property was measured at the current densities of 0.01, 0.02, 0.04 and 0.08 mA cm^{-2} with cutoff voltage of −0.2 to 0.8 V. The electrochemical impedance spectroscopy (EIS) was carried out in the frequency range of 10^5–0.001 Hz at a 5 mV amplitude referring to the open circuit potential. The charge storage capacitance of the supercapacitors was studied by cyclic voltammetry (CV) at a series of scan rates and GCD at different current densities. The long term cycling stability behavior of the supercapacitors was assessed using GCD measurements with a potential range between −0.2 and 0.8 V for 3000 cycles.

3. Results and discussion

3.1. Characteristics of the hybrid multilayer thin films

In order to get better adsorption efficiency of PANI, the pH value of PANI was adjusted to 2.6–2.9 by adding several drops of 1 M HCl, as monitored by the UV–vis spectra (Fig. S3). The pH value of GO and PEDOT:PSS was adjusted to 2.5–7 for PANI to remain stable during the assembly. It should be noted that the PANI dispersions were not stable below pH 2.5 and above pH 7, at these conditions,

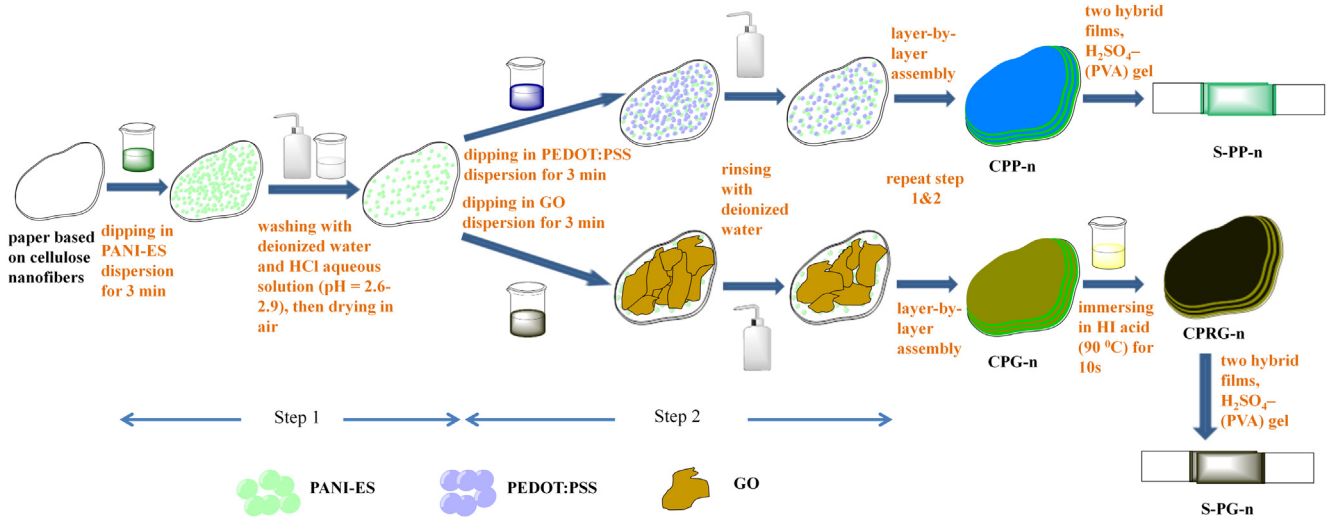

Scheme 1. Schematic illustration of the LbL assembly processes used to prepare the CPP-*n*, CPG-*n* multilayer films and the preparation of the flexible supercapacitors.

polymer would precipitate within a few hours of preparation, so such conditions could not be used to build up LbL multilayer films.

Successful LbL assembly was confirmed via UV–vis spectroscopy (Fig. 1a, b). The inset of Fig. 1a, b shows the absorbance of PANI layer (828 nm) nearly linearly proportional to the number of self-assembled layers. It is difficult for us to confirm the GO and PEDOT:PSS were successfully assembled from the UV–vis spectroscopy, because the peaks of GO and PEDOT:PSS were covered by the absorbance of CNFs and PANI, respectively. We hypothesize that the successful assembly is primarily driven by electrostatic interactions between positively charged PANI particles and negatively charged GO nanosheets (or PEDOT:PSS particles). To test this hypothesis, we carried out LbL assembly using only PANI (without GO and PEDOT:PSS suspension), as expected, there was no observable growth. UV–vis absorption spectra of CPRG-8 hybrid paper (at 266 nm, the characteristic absorption peak of RGO, Fig. 1c) exhibits the successful reduction of GO.

The surface chemistry of CPRG-8 and CPP-8 multilayer films electrodes was further investigated using XPS spectra. The survey scan spectra of CPRG-8 and CPP-8 multilayer films (Fig. S4a, b) show that a considerable amount of oxygen and nitrogen functional groups within the films. These I peaks in the spectrum of CPRG-8 come from the residual HI acid and I_2. It is obvious that the S 2p peak in the spectrum of CPP-8 is derived from PEDOT:PSS. The N1s spectrum (Fig. 1d, e) shows that the most nitrogen atoms are in the form of amine (–NH–) centered at 399.9 eV in benzenoid amine or amide groups [35]. Two small additional peaks suggest that some nitrogen atoms are imine groups (=NH–) centered at 398.2 eV and positively charged nitrogen groups (N^+) centered at 401.1 eV [2,36].

Fig. 1f shows XRD patterns of CNFs film, CPG-8 film, CPRG-8 film and CPP-8 film. The diffractogram shows two peaks at around 2θ 15.6° and 22.5° (the diffraction peaks of GO, RGO, PANI and PEDOT:PSS are not detected), which is very similar to the diffractogram of typical cellulose I crystalline structure [37]. Due to the I crystalline structure of cellulose, CNFs have the properties of low CTE, high mechanical strength and excellent flexibility. The diffractogram indicates that CNFs film also has the I crystalline structure of cellulose and LbL assembly process does not destroy the structure. The CPRG-8 film still has the typical cellulose I crystalline structure, though it has been immersed in HI acid (90 °C) for 10 s when GO nanosheets were reduced to RGO nanosheets.

The surface and cross-section morphology of CPRG-8 film and CPP-8 film were examined by SEM observations. Fig. 2a, b shows that the surface of CPRG-8 film is rugged, while the surface of CPP-8 film is smooth. The texture of CPRG-8 film may act as internal electrolyte nano-reservoirs when it used as electrodes in supercapacitors. The cross-section morphology of CPRG-8 and CPP-8 films (Fig. 2c, d) is different, too. There are a lot of pores on the CPRG-8 film' cross-section, on the contrary, the cross-sectional microstructure of CPP-8 film is compact. The interspace in the CPRG-8 film can provide channels for ions to diffuse to the electrochemical active materials, which will improve the performance of supercapacitors fabricated by the CPRG-8 film electrodes.

3.2. Capacitive performance

Fig. 3a, b exhibits the CV curves of S-PG-8 and S-PP-8 with a potential range between −0.2 and 0.8 V at different scan rates from 2 to 100 mV s^{-1}. The CV curves for S-PG-8 exhibit a similar rectangular capacitive behavior with a small portion of pseudocapacitive redox peaks, while the CV curves for S-PP-8 are somehow distorted. The rectangular and symmetric shapes of the CV curves for S-PG-8 indicate that the electrodes have excellent electrical double layer (EDL) capacitive behavior with very rapid current response on voltage reversal associated with EDL capacitive behavior of RGO. The slighter distortion of CV curves for S-PG-8 results from pseudocapacitive property of PANI and the surface functional groups attached to the surface of RGO such as carboxylic acid groups, which makes a contribution to improving the capacitance of supercapacitors [38]. Owing to RGO and PANI, S-PG-8 has the merits of both EDL capacitance and pseudocapacitance. In other words, the CV curves for S-PG-8 demonstrate that both of RGO and PANI contribute to the specific capacitance of the composite. However, due to the fact that both PANI and PEDOT are ECPs and the existence

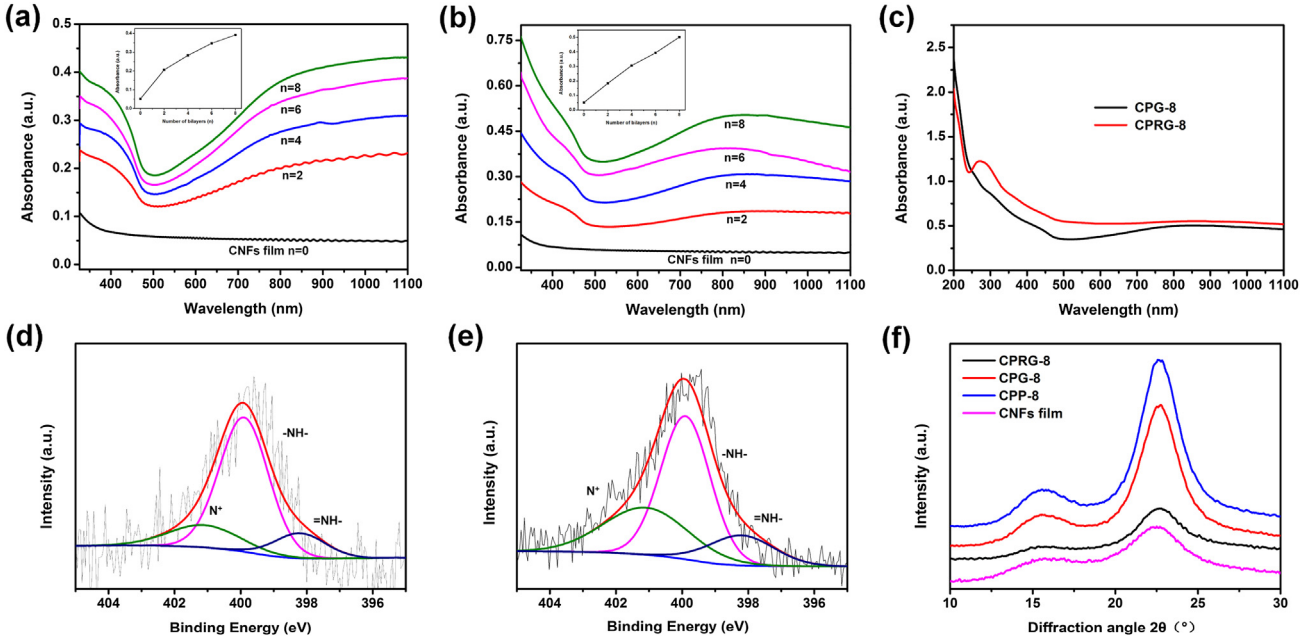

Fig. 1. UV/vis absorbance spectra's of CPP-*n* multilayer films (a) and CPG-*n* multilayer films (b), insets show the nearly linearly proportional between the absorbance at the characteristic peak. (c) UV/vis absorbance spectra's of CPG-8 multilayer film and CPRG-8 multilayer film. High-resolution XPS N1 spectra of CPRG-8 multilayer films (d) and CPP-8 multilayer films (e). (f) XRD patterns of CNFs film, CPG-8 film, CPRG-8 film and CPP-8 film.

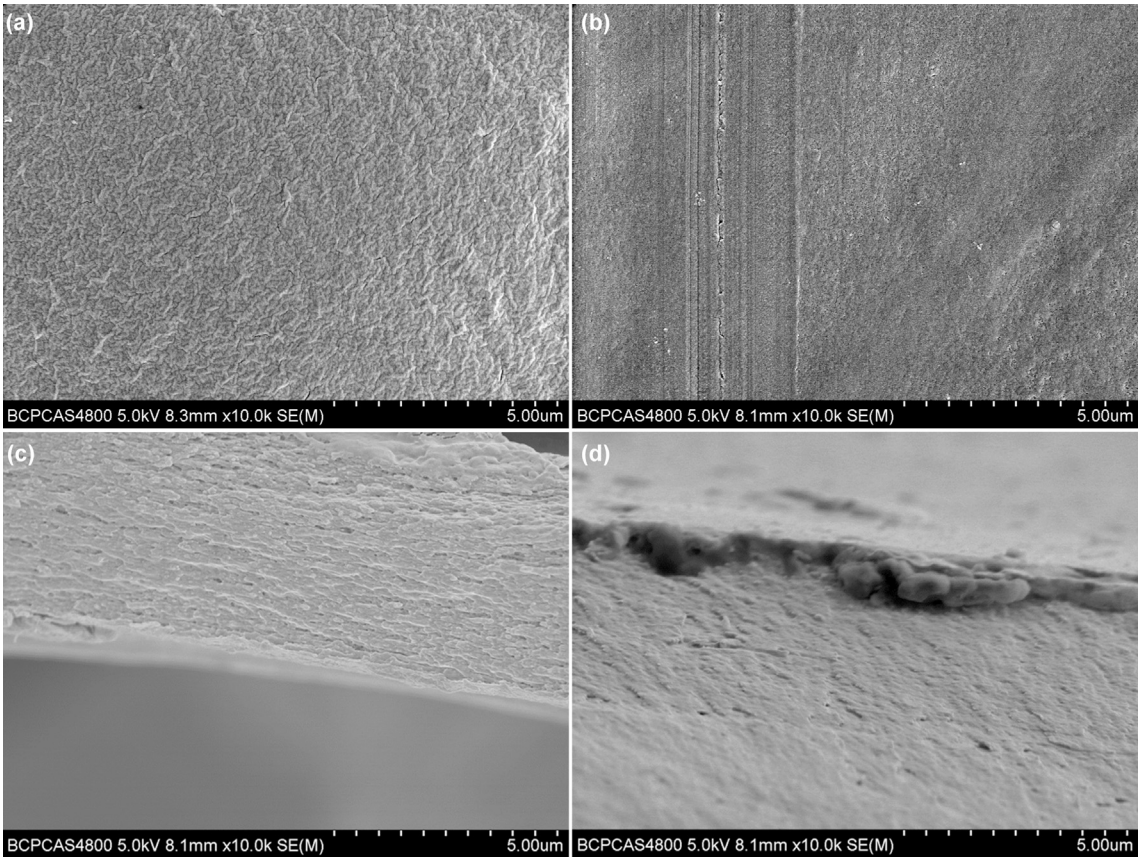

Fig. 2. SEM images of (a) the surface of CPRG-8 film, (b) the surface of CPP-8 film, (c) the cross-section of CPRG-8 film and (d) the cross-section of CPP-8 film.

of redox states in the presence of dopants, the CV curves for S-PP-8 exhibit obvious portion of pseudocapacitive redox peaks.

Owing to the very low mass loading of active material on the multilayer thin film electrodes, most electrodes achieve very high gravimetric capacitance values, but poor areal capacitance values [4]. Considering the real applications, areal capacitance values (F cm^{-2}) are more appropriate to assess the capacitance performance of thin film supercapacitor, although the gravimetric capacitance values (F g^{-1}) have always been used to evaluate the performance for supercapacitor [39]. To evaluate the charge storage capacitance of the device, the areal capacitance was calculated using CV curves obtained at different scan rates (Fig. 3e). At a low scan rate of 2 mV s^{-1}, the S-PG-8 could deliver approximately 5.72 mF cm^{-2}, the value is two times that of S-PP-8 (2.91 mF cm^{-2}). At a fast sweep rate of 500 mV s^{-1}, the device of S-PG-8 still obtains a capacitance of 0.16 mF cm^{-2}, but the capacitance of S-PP-8 is just 0.058 mF cm^{-2}. With the decrease of scan rate, the ratio of S-PG-8′ capacitance to S-PP-8′ capacitance is first increased and then decreased (Fig.3e, inset). The reasons for the change of the ratio may be that the internal electrolyte nano-reservoirs (CPRG-8 film and adsorbed electrolyte) significantly decrease the distance of electrolyte ions diffusion and improve accessible surface area of electrode material with electrolyte and the interspace between RGO nanosheets layers and PANI nanowires effectively facilitate diffusion of electrolyte ions. However, at low scan rates, there is enough time for the current accumulating process. Therefore, the penetration of electrolyte ions from electrolyte source to active surface on the electrode of S-PP-8 will be a lot deeper, which enabled pseudocapacitive property of PANI and PEDOT:PSS in S-PP-8 to be put into good use, thereby resulting in a trend that the areal capacitance of S-PP-8 catch up with that of S-PG-8. In short, diffusion of electrolyte ions plays a decisive part in the capacitance improvement at a fast sweep rate, but if there is enough time for the electrolyte ions diffusing into S-PP-8, pseudocapacitive property occupies a dominant.

Fig. 3c, d shows the GCD curves of S-PG-8 and S-PP-8. The near triangular shape of the curves for S-PG-8 indicates that the composites have good capacitive behaviors and rapid current–voltage response. However, the charge and discharge curves are not perfectly straight line due to the presence of pseudocapacitance, which might be associated with the existence of PANI and oxygen containing functional groups of RGO. The distorted triangular shape of GCD curves for S-PP-8 mainly attributes to pure pseudocapacitance [40]. The GCD curves for S-PG-8 show a lower IR drop during the discharge compared to that of the S-PP-8, clearly indicating the better conductivity of the active materials in S-PG-8. The capacitances obtained through CV data are similar to those from the GCD measurement, as shown in Fig. S5 in the ESI. With the decrease of current density, the areal capacitances of S-PP-8 is up to 4.37 mF cm^{-2} at a current density of 0.00405 mA cm^{-2}, which is closer and closer with the capacitance performance of S-PG-8. The areal capacitance of S-PG-8 is 5.86 mF cm^{-2} at a current density of 0.0043 mA cm^{-2}, and S-PP-8 also exhibits an excellent areal capacitance of 4.22 mF cm^{-2} at the same current density.

The electrochemical performance of S-PG-8 and S-PP-8 were further examined by the EIS analysis in a frequency range of 10^5–0.001 Hz, are shown as Nyquist plots in Fig. 3f. In the high-frequency region, the real axis intercept is the equivalent series resistance (ESR). Owing to only a few active materials on the multilayer thin film electrodes, the ESR values of both S-PG-8 and

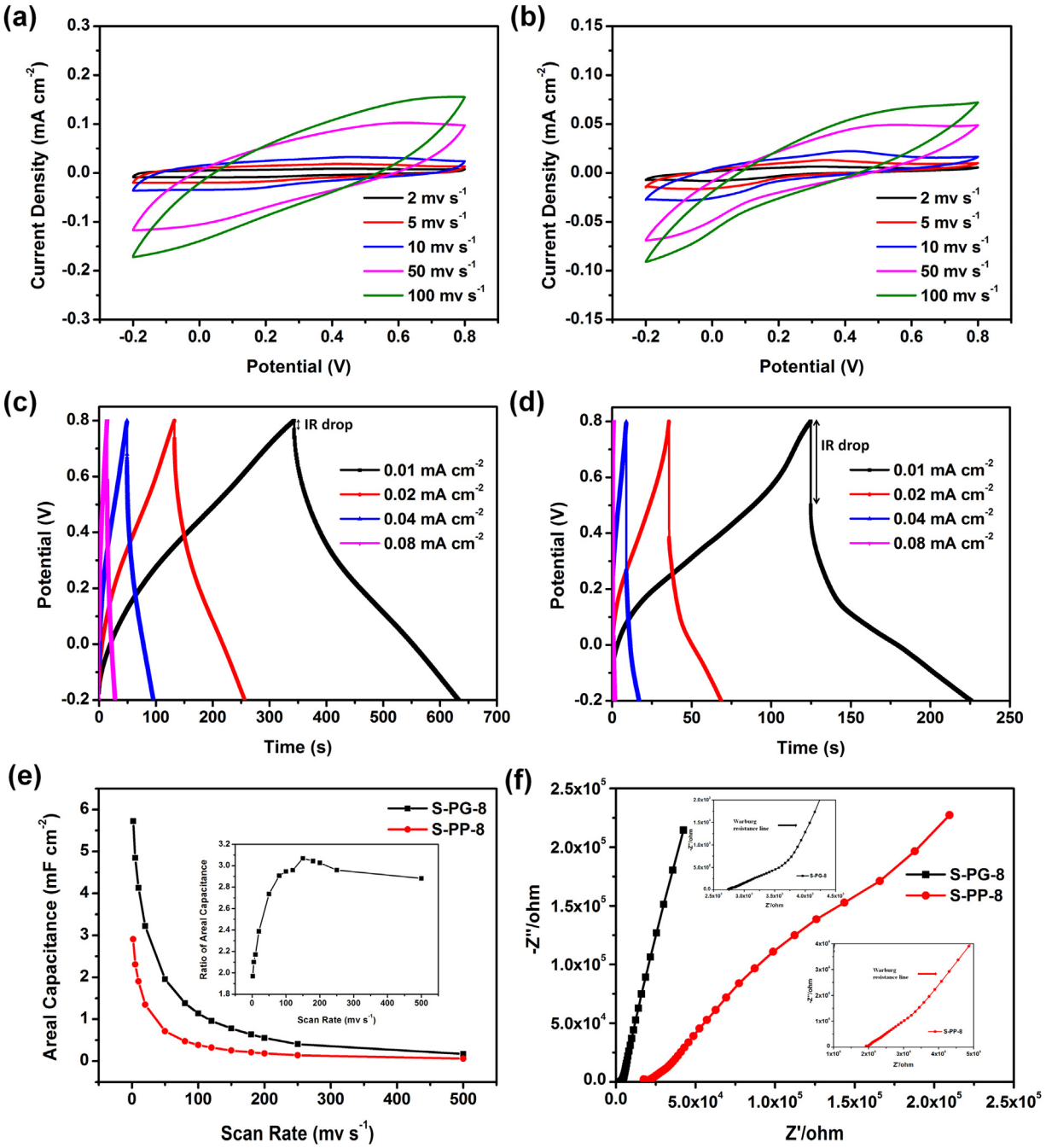

Fig. 3. Typical CV curves of S-PG-8 (a), S-PP-8 (b) device at different scan rates. Typical galvanostatic charge–discharge curves of S-PG-8 (c), S-PP-8 (d) device at different current densities. (e) The areal capacitance of S-PG-8 and S-PP-8 device at different scan rate. The inset shows the ratio of S-PG-8' capacitance to S-PP-8' capacitance is first increased and then decreased. (f) EIS with sweep frequency of 10^5–0.001 Hz. The inset shows the magnified high-frequency and medium-frequency regions.

S-PP-8 are very high. The ESR value of S-PP-8 is higher due to the lower conductivity of PEDOT (compared with RGO), which agree with the results obtained from GCD curves. In the medium-frequency region, the inclined Warburg resistance line with a slope of about 45° above the knee frequency is representative of the diffusion of electrolyte ions within porous electrodes [41,42]. The projected length of the Warburg curve on the real impedance axis characterizes the ion penetration process [42]. The Warburg length of the S-PG-8 is extremely shorter than that of S-PP-8 indicates the fast electrolyte ion diffusion in the electrode of CPRG-8, which corresponds with the CV results. At low frequencies region, S-PG-8 device exhibits a straight and nearly vertical line indicates the ideal capacitive behavior of the device. The knee frequencies of the S-PG-8 and S-PP-8 device are 3162 and 56.2 mHz, respectively. Generally, a higher knee frequency corresponds to a better rate performance [41], which also indicates the more excellent electrochemical performance of S-PG-8.

Fig. 4a shows the long term cycling stability behavior of flexible thin film supercapacitors that were examined using GCD with a potential range between −0.2 and 0.8 V. After 1000 times of cycling, the capacitance of S-PG-8 is 78.3% retention of the initial capacitance. After more 2000 times of cycling, the capacitance of S-PG-8 demonstrates a good cycling stability with only a 4.6% fall in the capacitance of 1000 times of cycling (Fig. 4a, inset). Interestingly, the

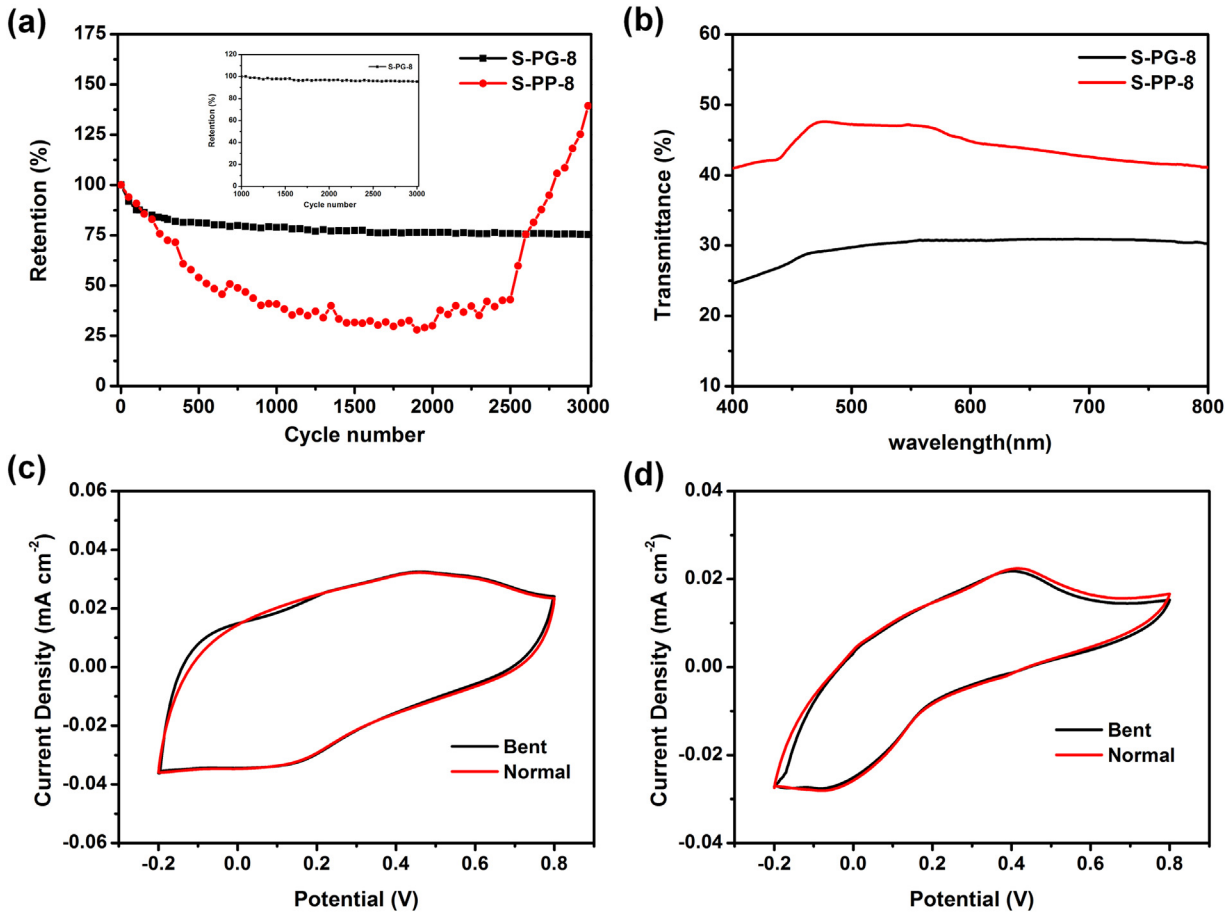

Fig. 4. (a) Cycling stability of S-PG-8 and S-PP-8 device over 3000 cycles. The inset shows the good cyclic stability of S-PG-8 after 1000 times of cycling. (b) Transmission of S-PG-8 and S-PP-8 device. Comparison of CV curves at 10 mV s^{-1} for S-PG-8 (c) and S-PP-8 (d) device tested under normal and bent state.

capacitance of S-PP-8 decreased to 27.9% after 1900 cycles and sharply increased to 139.4% from 2500 times of cycling to 3000 times of cycling, which indicates the stability of S-PG-8 is radically improved by RGO when compared with that of only ECPs. From Fig. 4a, S-PP-8 shows a less retention than S-PG-8 before 2500 cycles, but the former shows a higher retention than the latter after 2500 cycles. The reason for this may be that the diffusion of electrolyte ions from electrolyte source to the electrochemical active materials on the electrode of S-PG-8 is faster than that of S-PP-8 which has been demonstrated by the results obtained from the SEM images and the characteristic of areal capacitance. According to our results, the PEDOT:PSS layer played an important role in reducing the inner resistance and improving the capacitance of S-PP-8. However, because the diffusion of electrolyte ions is a slow process in S-PP-8, most of PEDOT:PSS is inoperative at first. On the contrary, the faster and deeper diffusion of electrolyte ions in S-PG-8 enables most of the electrochemical active materials to be used and the excellent EDL capacitive behavior of RGO plays an important role for the stability, so S-PG-8 shows a higher retention than S-PP-8 before 2500 cycles. After 2500 cycles, with the penetration of electrolyte ions of S-PP-8 becoming deeper and deeper, pseudocapacitive property of PANI and PEDOT:PSS in S-PP-8 will be put into good use, thereby resulting in S-PP-8 shows a higher retention than S-PG-8.

3.3. Transparency and flexibility test

Although S-PP-8' electrochemical performance is not as good as S-PG-8's, its transparency is better than S-PG-8's, which is pivotal for a transparent flexible electrochromic device. Compared with S-PP-8, the transmittance of S-PG-8 is lower at 550 nm, as a result of GO' color (dark brown). Transmittance of S-PG-8 and S-PP-8 are about 30.6% and about 47.1% (at 550 nm), respectively (Fig. 4b). In addition, S-PG-8 and S-PP-8 also exhibit highly flexible, and the capacitive performances of S-PG-8 and S-PP-8 are almost no change obviously in the bent states (Fig. 4c, d).

4. Conclusions

In conclusion, a simple method is provided to prepare hybrid multilayer thin film electrodes using transparent CNFs paper as the substrates by nano-scale blending LbL assembly based on electrostatic interactions. And then, two different transparent flexible thin film supercapacitors S-PG-8 and S-PP-8 were successfully fabricated by these thin film electrodes. With electrochemical testing, we found that the CPRG-8 electrodes can effectively facilitate diffusion of electrolyte ions, and the supercapacitors fabricated by CPRG-8 exhibits more excellent electrochemical performance, benefiting from the EDL capacitive behavior of RGO and pseudocapacitive property of PANI synergistically. The areal capacitance of S-PG-8 is up to 5.86 mF cm^{-2} at a current density of 0.0043 mA cm^{-2}, and at the same current density the areal capacitance of S-PP-8 is 4.22 mF cm^{-2}. S-PG-8 also exhibits good cyclic stability. However, the capacitance of S-PP-8 is unstable in the long term cycling. The transmittance of S-PP-8 is about 47.1% (at 550 nm), while that of S-PG-8 is about 30.6% (at 550 nm). The better transparency of S-PP-8 is pivotal for transparent flexible device. The

transparent flexible thin film supercapacitors also exhibit excellent bending stability. Our work provides a method to prepare hybrid electrodes with diverse microstructures for future flexible supercapacitors based on transparent CNFs paper.

Appendix A. Supplementary data

Supplementary data related to this article can be found at http://dx.doi.org/10.1016/j.jpowsour.2013.09.130.

References

[1] L. Yuan, B. Yao, B. Hu, K. Huo, W. Chen, J. Zhou, Energy Environ. Sci. 6 (2013) 470–476.
[2] T. Lee, T. Yun, B. Park, B. Sharma, H.K. Song, B.S. Kim, J. Mater. Chem. 22 (2012) 21092–21099.
[3] X. Guo, J. Lin, H. Chen, X. Zhang, Y. Fan, J. Luo, X. Liu, J. Mater. Chem. 22 (2012) 17176–17182.
[4] Y.Y. Horng, Y.C. Lu, Y.K. Hsu, C.C. Chen, L.C. Chen, K.H. Chen, J. Power Sources 195 (2010) 4418–4422.
[5] W. Hu, S. Chen, Z. Yang, L. Liu, H. Wang, J. Phys. Chem. B 115 (2011) 8453–8457.
[6] J. Ge, G. Cheng, L. Chen, Nanoscale 3 (2011) 3084–3088.
[7] S. Cospito, B.C. De Simone, A. Beneduci, D. Imbardelli, G. Chidichimo, Mater. Chem. Phys. 140 (2013) 431–434.
[8] K. Wang, H. Wu, Y. Meng, Y. Zhang, Z. Wei, Energy Environ. Sci. 5 (2012) 8384–8389.
[9] A.R. Rathmell, B.J. Wiley, Adv. Mater. 23 (2011) 4798–4803.
[10] H. Zhu, Z. Xiao, D. Liu, Y. Li, N.J. Weadock, Z. Fang, J. Huang, L. Hu, Energy Environ. Sci. 6 (2013) 2105–2111.
[11] T. Saito, S. Kimura, Y. Nishiyama, A. Isogai, Biomacromolecules 8 (2007) 2485–2491.
[12] A. Isogai, T. Saito, H. Fukuzumi, Nanoscale 3 (2011) 71–85.
[13] D.M. DeLongchamp, M. Kastantin, P.T. Hammond, Chem. Mater. 15 (2003) 1575–1586.
[14] L.C.P. Almeida, V. Zucolotto, R.A. Domingues, T.D.Z. Atvars, A.F. Nogueira, Photochem. Photobiol. Sci. 10 (2011) 1766–1772.
[15] J.B. Sim, H.H. Yang, M.J. Lee, J.B. Yoon, S.M. Choi, Appl. Phys. A: Mater. Sci. Process. 108 (2012) 305–311.
[16] C.H.B. Silva, N.A. Galiote, F. Huguenin, E. Teixeira-Neto, V.R.L. Constantino, M.L.A. Temperini, J. Mater. Chem. 22 (2012) 14052–14060.
[17] L. Zhang, H. Ma, F. Cao, J. Gong, Z. Su, J. Polym. Sci. Part A: Polym. Chem. 50 (2012) 912–917.
[18] J. Tarver, Y.L. Loo, Chem. Mater. 23 (2011) 4402–4409.
[19] L. Shao, J.W. Jeon, J.L. Lutkenhaus, Chem. Mater. 24 (2012) 181–189.
[20] S. Adibi, N. Adibi, R. Malekfar, S. Davatolhagh, Eur. Phys. J. Appl. Phys. 61 (2013).
[21] D. Alemu, H.Y. Wei, K.C. Ho, C.W. Chu, Energy Environ. Sci. 5 (2012) 9662–9671.
[22] H. Huang, S. Lu, X. Zhang, Z. Shao, Soft Matter 8 (2012) 4609–4615.
[23] G. Jiang, A. Baba, R. Advincula, Langmuir 23 (2007) 817–825.
[24] K. Sheng, H. Bai, Y. Sun, C. Li, G. Shi, Polymer 52 (2011) 5567–5572.
[25] X. Zhang, Z. Sui, B. Xu, S. Yue, Y. Luo, W. Zhan, B. Liu, J. Mater. Chem. 21 (2011) 6494–6497.
[26] C.X. Guo, C.M. Li, Energy Environ. Sci. 4 (2011) 4504–4507.
[27] T.J. Dawidczyk, M.D. Walton, W.S. Jang, J.C. Grunlan, Langmuir 24 (2008) 8314–8318.
[28] P. Andersson, R. Forchheimer, P. Tehrani, M. Berggren, Adv. Funct. Mater. 17 (2007) 3074–3082.
[29] T. Saito, Y. Nishiyama, J.L. Putaux, M. Vignon, A. Isogai, Biomacromolecules 7 (2006) 1687–1691.
[30] J.C. Chiang, A.G. Macdiarmid, Synth. Met. 13 (1986) 193–205.
[31] K.S. Ryu, B.W. Moon, J. Joo, S.H. Chang, Polymer 42 (2001) 9355–9360.
[32] V.C. Tung, M.J. Allen, Y. Yang, R.B. Kaner, Nat. Nanotechnol. 4 (2009) 25–29.
[33] S. Pei, J. Zhao, J. Du, W. Ren, H.M. Cheng, Carbon 48 (2010) 4466–4474.
[34] C. Meng, C. Liu, L. Chen, C. Hu, S. Fan, Nano Lett. 10 (2010) 4025–4031.
[35] M.M. Castillo-Ortega, I. Santos-Sauceda, J.C. Encinas, D.E. Rodriguez-Felix, T. del Castillo-Castro, F. Rodriguez-Felix, J.L. Valenzuela-Garcia, L.S. Quiroz-Castillo, P.J. Herrera-Franco, J. Mater. Sci. 46 (2011) 7466–7474.
[36] M.N. Hyder, S.W. Lee, F.C. Cebeci, D.J. Schmidt, Y. Shao-Horn, P.T. Hammond, ACS Nano. 5 (2011) 8552–8561.
[37] S.J. Eichhorn, Soft Matter 7 (2011) 303–315.
[38] J. Zhang, Y. Yu, L. Liu, Y. Wu, Nanoscale 5 (2013) 3052–3057.
[39] M.D. Stoller, R.S. Ruoff, Energy Environ. Sci. 3 (2010) 1294–1301.
[40] L. Yuan, X. Xiao, T. Ding, J. Zhong, X. Zhang, Y. Shen, B. Hu, Y. Huang, J. Zhou, Z.L. Wang, Angew. Chem. Int. Ed. 51 (2012) 4934–4938.
[41] Z. Weng, Y. Su, D.W. Wang, F. Li, J. Du, H.M. Cheng, Adv. Energy Mater. 1 (2011) 917–922.
[42] M. Hughes, G.Z. Chen, M.S.P. Shaffer, D.J. Fray, A.H. Windle, Chem. Mater. 14 (2002) 1610–1613.